Journal of Magnetic Resonance **145,** 84–94 (2000)
doi:10.1006/jmre.2000.2069, available online at http://www.idealibrary.com on IDEAL®

Spin Relaxation Measurements Using First-Harmonic Out-of-Phase Absorption EPR Signals: Rotational Motion Effects

V. A. Livshits* and D. Marsh

*Abteilung Spektroskopie, Max-Planck-Institut für biophysikalische Chemie, D-37070, Göttingen, Germany; and *Centre of Photochemistry, Russian Academy of Sciences, 117427, Moscow, Russian Federation*

Received October 22, 1999; revised February 14, 2000

A recent survey of nonlinear continuous-wave (CW) EPR methods revealed that the first-harmonic absorption EPR signal, detected 90° out of phase with respect to the Zeeman modulation (V_1'-EPR), is the most appropriate for determining spin–lattice relaxation enhancements of spin labels (V. A. Livshits, T. Páli, and D. Marsh, 1998, *J. Magn. Reson.* **134, 113–123). The sensitivity of such V_1'-EPR spectra to molecular rotational motion is investigated here by spectral simulations for nitroxyl spin labels, over the entire range of rotational correlation times. Determination of the effective spin–lattice relaxation times is less dependent on rotational mobility than for other nonlinear CW EPR methods, especially at a Zeeman modulation frequency of 25 kHz which is particularly appropriate for spin labels. This relative insensitivity to molecular motion further enhances the usefulness of the V_1'-EPR method. Calibrations of the out-of-phase to in-phase spectral intensity (and amplitude) ratios are given as a function of spin–lattice relaxation time, for the full range of spin-label rotational correlation times. Experimental measurements on spin labels in the slow, intermediate, and fast motional regimes of molecular rotation are used to test and validate the method.**

INTRODUCTION

Spin–lattice relaxation of nitroxide spin labels currently finds increasing application in membrane biophysics. Structural information is obtained by measuring relaxation enhancements induced by paramagnetic relaxation agents, and sensitivity to slow dynamic processes is also very much enhanced (*1–3*). It is well known that information on spin relaxation rates may be obtained from progressive saturation experiments. These experiments use the conventional V_1-EPR spectra detected in phase with the first harmonic of the Zeeman modulation field. On the other hand, the absorption V_2'-EPR spectra of spin labels detected at the second modulation harmonic, in phase quadrature with the modulation field (i.e., saturation transfer EPR), are also used to measure spin–lattice relaxation enhancements (*3*). These include relaxation enhancements induced by Heisenberg spin exchange or by dipole–dipole interactions with fast-relaxing paramagnetic species.

Continuous-wave (CW) EPR experiments, as compared to pulse measurements, have the advantage of relative accessibility and high concentration sensitivity. Therefore, it is useful to explore new nonlinear CW approaches to the determination of spin relaxation rates of spin-labeled molecules. Of these, the V_2' saturation transfer EPR spectra, although being sensitive to T_1, are also very sensitive to molecular motion (*4*) and to T_2 relaxation (*5*). In comparison, conventional CW progressive saturation parameters are less sensitive to T_1, and also they are dependent directly on T_2.

Recently, we proposed the use of the out-of-phase first-harmonic EPR absorption signals (V_1') for determining spin–lattice relaxation enhancements (*6*). This V_1'-EPR signal was first suggested by Hyde and Thomas (*7*) as a T_1-sensitive nonlinear EPR display. In Ref. (*6*) we showed both theoretically and experimentally that the V_1'-EPR amplitudes or double integrals are more sensitive to T_1 and less dependent on T_2 than are conventional in-phase V_1-EPR spectra. A survey of nonlinear CW EPR methods suggested that first-harmonic out-of-phase V_1'-EPR was the method of choice for determining T_1 relaxation enhancements of spin labels. These results, however, were obtained in the absence of molecular motion and for a single-line spectrum.

For the practical application of this new CW approach, it is important to investigate the dependence of the T_1- and T_2-sensitive spectral parameters of the V_1'-EPR spectra on the dynamics of rotational motion. A dependence is to be expected for nitroxide spin labels under conditions of partial saturation. This is because molecular rotation induces spectral diffusion of microwave saturation and provides a mechanism for transverse spin relaxation by modulation of the Zeeman and hyperfine anisotropies. The aim of the present work is to extend the capability of out-of-phase first-harmonic V_1'-EPR measurements for determining the T_1 relaxation times of spin labels to the whole range of rotational correlation times. Calibrations are given for the T_1-sensitive parameters of the V_1'-EPR spectra at different rotational mobilities. The applicability of this approach is demonstrated experimentally for spin labels in viscous glycerol–water mixtures in the rapid, intermediate, and slow motional regimes.

MATERIALS AND METHODS

The spin label TEMPONE (4-oxo-2,2,6,6-tetramethylpiperidine-*N*-oxyl) was obtained from Eastman Kodak (Rochester, NY). Maleimide spin label, 3-maleimidoproxyl (5-MSL), was

1090-7807/00 $35.00

from Sigma (St. Louis, MO). The TEMPONE spin label was used at a concentration of 3×10^{-4} M in glycerol–water solutions. All samples were saturated with argon.

EPR spectra were recorded on a Varian Century Line, or on a Bruker EMX, 9-GHz EPR spectrometer. Magnetic field modulation frequencies of 100 and 25 kHz were used, and a static field scan range of 100 to 200 G (depending on the spectral extent at high microwave power). Samples of 5 mm length were contained in sealed 0.7- or 1-mm-i.d. glass capillaries. These were accommodated within a standard quartz EPR tube that contained light silicone oil for thermal stability. The samples were centered vertically in the microwave cavity. The entire sample chamber was sealed under argon. The temperature of the samples was controlled by nitrogen gas flow through a quartz Dewar and was measured by a fine-wire thermocouple. This was located within the capillary in contact with the sample. Critical coupling conditions were used. Modulation phase settings were performed by the self-null method. Alternatively, a nonsaturating reference sample, a single crystal of copper sulfate, was used as described in Ref. (*6*). The root mean square microwave field, H_1, at the sample was calibrated by using a standard solution of peroxylamine disulfonate, as described in Ref. (*8*). Saturation transfer (V_2') EPR spectra, where appropriate, were recorded according to the standardized protocol described in Ref. (*9*).

Spectra were simulated according to the methods described under Theory. Principal values for the g and hyperfine tensors used in the simulations were $\mathbf{g} = (2.0089, 2.0061, 2.0027)$ and $\mathbf{A} = (6.0\text{ G}, 6.0\text{ G}, 34.0\text{ G})$, respectively. Double-integrated intensities were obtained by numerical integration of the simulated spectra over a magnetic field range of 200 G.

THEORY

Earlier, we obtained solutions of the modified Bloch equations for small field modulation amplitudes, h_m (*10*). This was done by using a strong jump diffusion model of molecular rotational motion. Integral equations were derived for the vector coefficients of $\vec{\mathbf{X}}_{1,1} = (u_{1,1}, v_{1,1}, z_{1,1})$ that define the magnetization components that are linear in h_m, and for the zero-order coefficients of $\vec{\mathbf{X}}_{0,0} = (u_{0,0}, v_{0,0}, z_{0,0})$ that correspond to magnetization components independent of h_m. These are given by the relations (*10*)

$$\hat{\mathbf{A}}_0 \cdot \vec{\mathbf{X}}_{0,0} = \vec{\mathbf{M}}_o + f_R \int \vec{\mathbf{X}}_{0,0} d\Omega \qquad [1]$$

$$\hat{\mathbf{A}}_1 \cdot \vec{\mathbf{X}}_{1,1} = f_R \int \vec{\mathbf{X}}_{1,1} d\Omega + (\hat{\gamma}/\gamma_e) \cdot \vec{\mathbf{X}}_{0,0}, \qquad [2]$$

where $f_R \equiv \tau_R^{-1}$ is the frequency of isotropic rotational reorientation, $\vec{\mathbf{M}}_o = M_o(0, 0, T_1^{-1})$, and $\Omega \equiv (\theta, \varphi)$ is the orientation of the static magnetic field relative to the magnetic principal axes. The modified Bloch equation matrix that appears in Eqs. [1] and [2] is given by

$$\hat{\mathbf{A}}_n = \begin{pmatrix} T_2^{-1} + f_R - in\omega_m \\ -\gamma_e[H - H_{res}(\theta, \varphi)] \\ 0 \end{pmatrix} \times \begin{matrix} \gamma_e[H - H_{res}(\theta, \varphi)] & 0 \\ T_2^{-1} + f_R - in\omega_m & -\gamma_e H_1 \\ \gamma_e H_1 & T_1^{-1} + f_R - in\omega_m \end{matrix} \qquad [3]$$

with

$$\hat{\gamma} = \begin{pmatrix} 0 & -\gamma_e & 0 \\ \gamma_e & 0 & 0 \\ 0 & 0 & 0 \end{pmatrix}, \qquad [4]$$

where H_{res} is the resonant field, and $f_m = \omega_m/2\pi$ is the modulation frequency. The resonant field, $H_{res}(\theta, \varphi)$, is angular dependent. It is determined by the g and hyperfine tensor anisotropies,

$$H_{res}(\theta, \varphi) = \frac{\hbar \omega_L}{\beta_e g(\theta, \varphi)} - M_I A(\theta, \varphi), \qquad [5]$$

where ω_L is the microwave frequency and M_I is the nuclear magnetic quantum number of the spin label. The tensor anisotropies are given by

$$g(\theta, \varphi) = g_{zz}\cos^2\theta + g_{xx} \cdot \sin^2\theta \cdot \cos^2\varphi + g_{yy}\sin^2\theta \cdot \sin^2\varphi \qquad [6]$$

$$A(\theta, \varphi) = (A_{zz}^2\cos^2\theta + A_{xx}^2\sin^2\theta\cos^2\varphi + A_{yy}^2\sin^2\theta\sin^2\varphi)^{1/2}, \qquad [7]$$

where the principal tensor components are $\mathbf{g} = (g_{xx}, g_{yy}, g_{zz})$ and $\mathbf{A} = (A_{xx}, A_{yy}, A_{zz})$.

The solution, $\vec{\mathbf{I}}_1 = \int \vec{\mathbf{X}}_{1,1} d\Omega$, of the integral Eq. [2] for the first harmonic is given in matrix form by (*10*)

$$\vec{\mathbf{I}}_1 = (\hat{\mathbf{E}} - \hat{\mathbf{J}}_1 f_R)^{-1} \cdot \vec{\mathbf{J}}_{10}, \qquad [8]$$

where $\hat{\mathbf{J}}_1 = \int \hat{\mathbf{A}}_1^{-1} d\Omega$ and $\vec{\mathbf{J}}_{10} = \int \hat{\mathbf{A}}_1^{-1} \cdot \hat{\gamma} \cdot \vec{\mathbf{X}}_{0,0} d\Omega$. The zero-order coefficients $\vec{\mathbf{X}}_{0,0}$ of the spin magnetization vector that are required for the $\vec{\mathbf{J}}_{10}$ integral are obtained from solution of Eq. [1]. These are given by (*10*)

$$\vec{\mathbf{X}}_{0,0} = \hat{\mathbf{A}}_0^{-1} \cdot [\vec{\mathbf{M}}_o + f_R(\hat{\mathbf{E}} - \hat{\mathbf{J}}_0 f_R)^{-1} \cdot \hat{\mathbf{J}}_0 \cdot \vec{\mathbf{M}}_o], \qquad [9]$$

where $\hat{\mathbf{J}}_0 = \int \hat{\mathbf{A}}_0^{-1} \cdot d\Omega$.

The lineshape of the first-harmonic out-of-phase absorption spectrum is finally given by

$$V'_1 = \mathrm{Im}\{V_{1,1}\}. \quad [10]$$

The conventional first-harmonic in-phase absorption spectrum is correspondingly given by

$$V_1 = \mathrm{Re}\{V_{1,1}\}. \quad [11]$$

In Eqs. [10] and [11], the value of $V_{1,1}$ is obtained from the solution of Eq. [8], which is expressed as $\vec{\mathbf{I}}_1 = (U_{1,1}, V_{1,1}, Z_{1,1})$. Inhomogeneous line broadening due to hyperfine interaction with methyl and environmental protons can be taken into account by convoluting the lineshapes of Eqs. [10] and [11] with a Gaussian function.

As noted in Ref. (*11*), use of a hyperfine resonance field given by Eq. [7] is an adiabatic approximation that is not applicable in the fast motion region ($\tau_R < 3 \times 10^{-9}$ s) (*12*). In this region, an additional contribution to the spin–spin relaxation rate, T_2^{-1}, arises from rotational modulation of the anisotropic Zeeman and hyperfine interactions. This can be determined by time-dependent perturbation theory in which the full spin Hamiltonian is used (*13*). The resulting expressions for the linewidths of the hyperfine components are written in the form

$$T_2^{-1}(M_I) = T_{2,0}^{-1} + A + BM_I + CM_I^2, \quad [12]$$

where $T_{2,0}^{-1}$ is the residual homogeneous broadening arising from mechanisms other than rotational motion. For isotropic rotational reorientation, the A, B, and C coefficients are (*13*)

$$A = \frac{4}{45}[(\Delta\omega)^2 + 3(\delta\omega)^2]\tau_R\left(1 + \frac{3}{4}\frac{1}{1+\omega_e^2\tau_R^2}\right) + \frac{7}{45}[(\Delta A)^2 + 3(\delta A)^2]\tau_R \times \left(\frac{1}{1+\omega_e^2\tau_R^2} + \frac{3}{7}\frac{1}{1+\omega_n^2\tau_R^2}\right) \quad [13]$$

$$B = \frac{8}{45}[\Delta\omega\Delta A + 3\delta\omega\delta A]\tau_R\left(1 + \frac{3}{4}\frac{1}{1+\omega_e^2\tau_R^2}\right) \quad [14]$$

$$C = \frac{4}{45}[(\Delta A)^2 + 3(\delta A)^2]\tau_R\left(1 - \frac{1}{8}\frac{1}{1+\omega_e^2\tau_R^2} - \frac{3}{8}\frac{1}{1+\omega_n^2\tau_R^2}\right), \quad [15]$$

where the tensor anisotropies $\Delta\omega = [g_{zz} - \frac{1}{2}(g_{xx} + g_{yy})]\beta_e H_0/\hbar$, $\delta\omega = \frac{1}{2}(g_{xx} - g_{yy})\beta_e H_0/\hbar$, $\Delta A = A_{zz} - \frac{1}{2}(A_{xx} + A_{yy})$, and $\delta A = \frac{1}{2}(A_{xx} - A_{yy})$ are in angular frequency units, and $\omega_n \approx \frac{1}{2}a_N$ is the nuclear Larmor frequency.

We have performed comparative simulations of the V'_1-EPR spectra by using different approximations. These are: (i) Eq. [12] with the expressions for the A, B, and C coefficients given by Eqs. [13]–[15] above; (ii) Eq. [12] and the above expressions for A, B, and C without the terms dependent on nuclear frequency (ω_n); and (iii) the adiabatic approximation, with the hyperfine field given by Eq. [7]. For fixed values of residual linewidth, $T_{2,0}^{-1}$, the spectral parameters used for determination of T_1 from the experimental spectra (i.e., the ratios of integrated intensities or low-field amplitudes of the out-of-phase and in-phase components) differ for the cases (i)–(iii). However, if separate values of $T_{2,0}^{-1}$ are determined for each model by simulations of the low-field component of the conventional (linear) experimental spectra, then the T_1 values obtained from the different approximations (i)–(iii) are very close to each other.

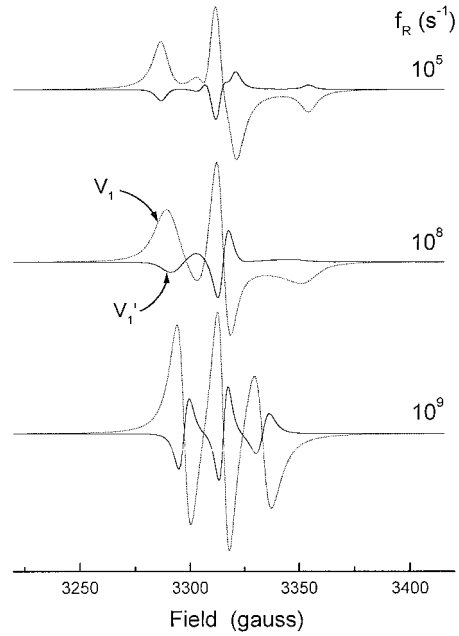

FIG. 1. Simulated first-harmonic out-of-phase V'_1 (solid lines)- and in-phase V_1 (dotted lines)-EPR spectra of nitroxide spin labels for different frequencies of isotropic rotation: $f_R = 10^5$, 10^8, and 10^9 s^{-1}. Modulation frequency, $\omega_m/2\pi = 100$ kHz; $H_1 = 0.4$ G; ΔH_0 $(=1/\gamma_e T_{2,0}) = 3.0$ G; $T_1 = 2 \times 10^{-6}$ s. The adiabatic approximation is used in these simulations.

RESULTS AND DISCUSSION

Simulations of Out-of-Phase First-Harmonic V'_1-EPR Spectra

Simulated first-harmonic in-phase and out-of-phase EPR spectra are given in Fig. 1. The simulations are for a nitroxide spin label undergoing isotropic rotation of different rates. In the case of moderate and high microwave saturation, the out-of-phase V'_1-EPR lineshape varies with rotational correlation time in a way similar to that of the in-phase V_1-EPR signal. This means that, in contrast to the second-harmonic out-of-phase spectra, the V'_1-EPR signals are not sensitive to slow rotational motions on the microsecond timescale.

The V'_1-EPR amplitudes decrease as H_1^2, with a decrease in microwave H_1-field intensity (see also Ref. *7*). At low satura-

tion, a sharp change in the lineshape occurs. In the rapid motion region, this change is similar to that for a single-line spectrum; cf. Ref. (*6*). If the condition $T_2/T_1 \ll 1$ is satisfied (where T_2^{-1} includes both the intrinsic and the rotationally induced spin–spin relaxation rate), T_1 can be estimated in a way similar to that for the "no motion" case (*6*). This method uses the microwave field amplitude, H_1^*, at which the transition in lineshape occurs.

Sensitivity of Out-of-Phase Intensities to T_1: Dependence on Rotational Frequency

More generally, the spin–lattice relaxation times may be determined from the integrated intensities, or amplitudes, of the V_1'-EPR spectra. In the absence of motion, useful T_1-sensitive parameters are dimensionless ratios of the double-integrated intensities, ρ_1', and of the low-field amplitudes, $\rho_1'(M_I = +1)$, for out-of-phase and in-phase spectra measured at the same value of H_1 (*6*). These ratios are used again here for quantitation of the spectra in the presence of rotational molecular motion. For integrated intensities and amplitudes, the ratios are, respectively,

$$\rho_1' = \frac{\int\int V_1' d^2H}{\int\int V_1 d^2H} \qquad [16]$$

$$\rho_1'(M_I = +1) = \frac{V_1'(M_I = +1)}{V_1(M_I = +1)}. \qquad [17]$$

In Eq. [17], $V_1'(M_I = +1)$ and $V_1(M_I = +1)$ are the maximum lineheights of the out-of-phase and in-phase spectra, respectively, in the low-field region. A local maximum (ignoring absolute sign) is well defined in the low-field region of the spectra, at all rotational frequencies (see Fig. 1). The T_1 dependences of the integrated intensity ratio are presented in Fig. 2, for modulation frequencies of 100 and 25 kHz, $H_1 = 0.5$ G, and different values of f_R. The values of the ρ_1' ratio have a nonmonotonic dependence on rotational frequency. They decrease with increasing f_R over the range 10^6–10^8 s^{-1}, but increase with increasing f_R, for $f_R \geq 10^8$ s^{-1}. Typical dependences of the intensity ratio ρ_1' and the absolute out-of-phase intensity $\int\int V_1' d^2H$ on f_R are given in Fig. 3, for $T_1 = 3$ μs and $H_1 = 0.5$ G. The dependence for the in-phase integral $\int\int V_1 d^2H$ is similar to that for the effective spin–spin relaxation rate, $1/T_2^{\text{eff}}$; see Ref. (*10*). On the other hand, that for the out-of-phase integral $\int\int V_1' d^2H$ is relatively weaker and multiphasic (see Fig. 3b). This latter dependence means that rotational motion affects the value of the out-of-phase magnetization through changes additional to those in the value of $1/T_2^{\text{eff}}$. This will be analyzed in more detail below.

Calibration of Integral Ratio T_1 Dependences

For all rotational frequencies in the range up to $f_R = 10^{11}$ s^{-1}, the dependence of the intensity ratio on T_1 can be fitted by an empirical expression of the same form as that used in the absence of molecular rotation (*6*),

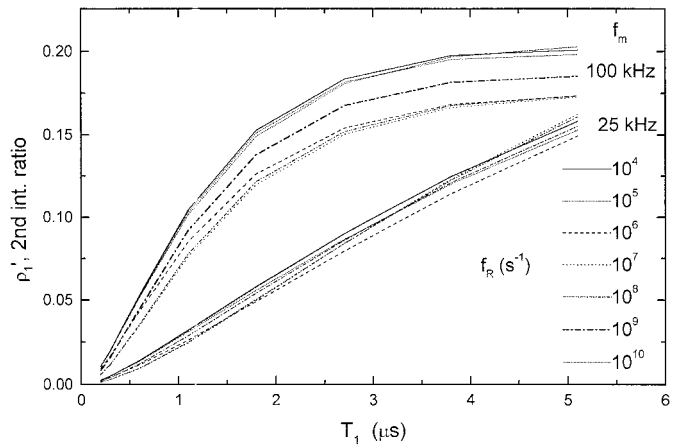

FIG. 2. Simulated dependences on spin–lattice relaxation time, T_1, of the ratio, ρ_1', of the integrated intensities of the first-harmonic out-of-phase spectra to those of the in-phase spectra, for different rotational frequencies, $f_R = 10^4$–10^{10} s^{-1}, and modulation frequencies, $\omega_m/2\pi$, of 100 and 25 kHz, with $H_1 = 0.5$ G, ΔH_0 $(=1/\gamma_e T_{2,0}) = 2.0$ G.

$$\rho_1' = \rho_1^{0'} + \frac{a_1' T_1^m}{1 + b_1' T_1^m}, \qquad [18]$$

where the fit parameters a_1', b_1', $\rho_1^{0'}$, and m depend on f_R, as well as on H_1, $T_{2,0}$, and ω_m. For $H_1 = 0.5$ G and $\omega_m/2\pi = 100$ kHz, satisfactory fits were obtained for all values of f_R and $T_{2,0}$ with $m = 2$. For a modulation frequency of $\omega_m/2\pi = 25$ kHz, fitted values of the exponent are $m = 1.3$–1.5, where the range of m applies to different T_1 intervals.

The fit parameters, a_1' and b_1', determine the slopes of the T_1 dependences in relaxation-enhancement experiments. Therefore it is important to know their variation with the rotational frequency f_R and transverse relaxation time, $T_{2,0}$ (or intrinsic linewidth, $\Delta H_0 = 1/\gamma_e T_{2,0}$). Typical dependences of these parameters on rotational frequency for different intrinsic linewidths are given in Figs. 4a and 4b. The absolute values of these parameters, and ranges of f_R, ΔH_0, and T_1 for which fits were performed, are given in Tables 1 and 2. These values were obtained with the adiabatic approximation, throughout the entire range of rotational frequencies. Their validity for the rapid motional region is established later, under Experimental Applications. The value of $\rho_1^{0'}$ is close to zero over most of the range of f_R. The dependences of the a_1' and b_1' parameters on f_R are both similar to that for ρ_1', at a modulation frequency of 100 kHz (see Fig. 3). The a_1' and b_1' parameters decrease approximately linearly with ΔH_0, but their absolute values change by only 30–40% when ΔH_0 changes from 0.5 to 3.0 G (see Figs. 4a and 4b). Moreover, this dependence becomes even weaker when approaching the region of maximum spectral diffusion rate ($f_R \approx 10^7$ s^{-1}), from both low and high rotational frequencies.

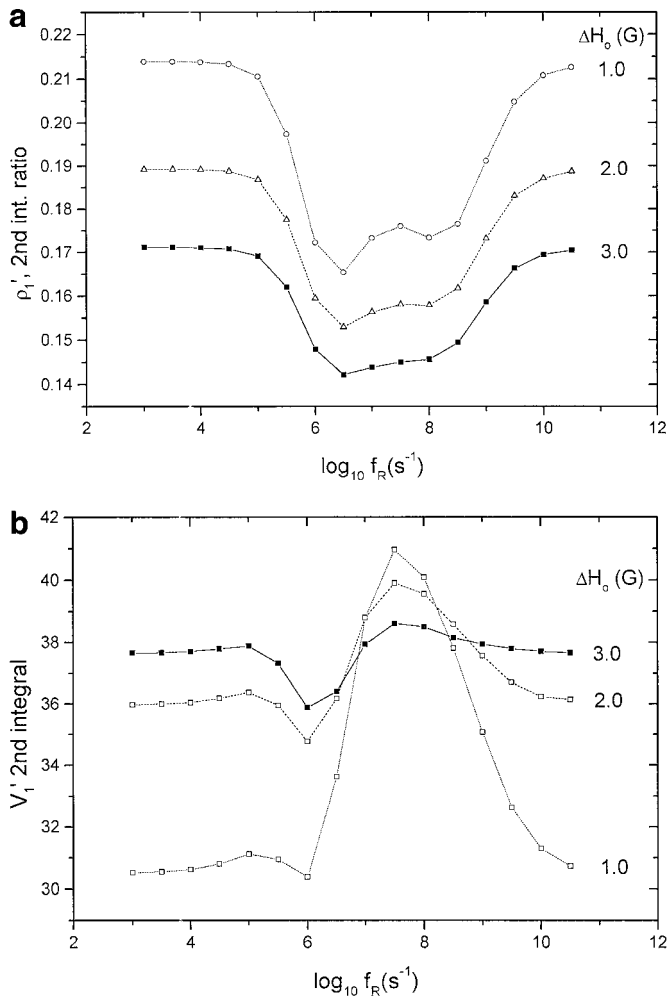

FIG. 3. Simulated dependences on rotational frequency, f_R, of (a) the ratio, ρ_1', of the integrated intensities of the out-of-phase and in-phase spectra, and (b) the integrated intensities of the V_1' signal, for different spin-packet widths, ΔH_0 $(=1/\gamma_e T_{2,0})$, a modulation frequency of 100 kHz, and $H_1 = 0.5$ G, $T_1 = 3 \times 10^{-6}$ s.

The dependence of the intensity ratios on rotational frequency, f_R, is substantially reduced at lower modulation frequencies. This is seen in Fig. 2 for $\omega_m/2\pi = 25$ kHz, in comparison with $\omega_m/2\pi = 100$ kHz. The exponent, m, is smaller at lower modulation frequencies ($m = 1.3$ for 25 kHz). Nevertheless, the dependences of the fit parameters a_1' and b_1' on f_R and $T_{2,0}$ are qualitatively similar to those for 100 kHz. The linear dependences of a_1' and b_1' on $T_{2,0}$ have smaller slopes at $\omega_m/2\pi = 25$ kHz. In addition, these differences are to a large extent compensated in the absolute values of the out-of-phase intensities, at the lower modulation frequency. Again, as for $\omega_m/2\pi = 100$ kHz, the dependence on $T_{2,0}$ becomes weaker when approaching the region of maximum spectral diffusion rate. Thus, the sensitivity of the first-harmonic intensity ratio to $T_{2,0}$ is weaker than that for the progressive saturation parameter (*10*), over the entire rotational frequency range. Moreover, it can be decreased even further by lowering the Zeeman modulation frequency.

As seen in Fig. 3a, the values of the integral parameter, ρ_1', are identical for no rotational motion and for very rapid rotation, even though the lineshapes are completely different for the two cases. This is because both spectral diffusion and the rotational contribution to the spin–spin relaxation rate are absent in these two limits.

Calibration of Amplitude Ratio T_1 Dependences

The dependence of the amplitude ratio, $\rho_1'(M_1)$, on T_1 can be fitted by an expression of the form

$$\rho_1'(M_1) = \rho_1^{0'}(M_1) + \frac{a_1'(M_1)T_1^m}{1 + b_1'(M_1)T_1^m}. \qquad [19]$$

This is similar to Eq. [18] for the integrated intensity ratio. Equation [19] applies over the whole range of rotational fre-

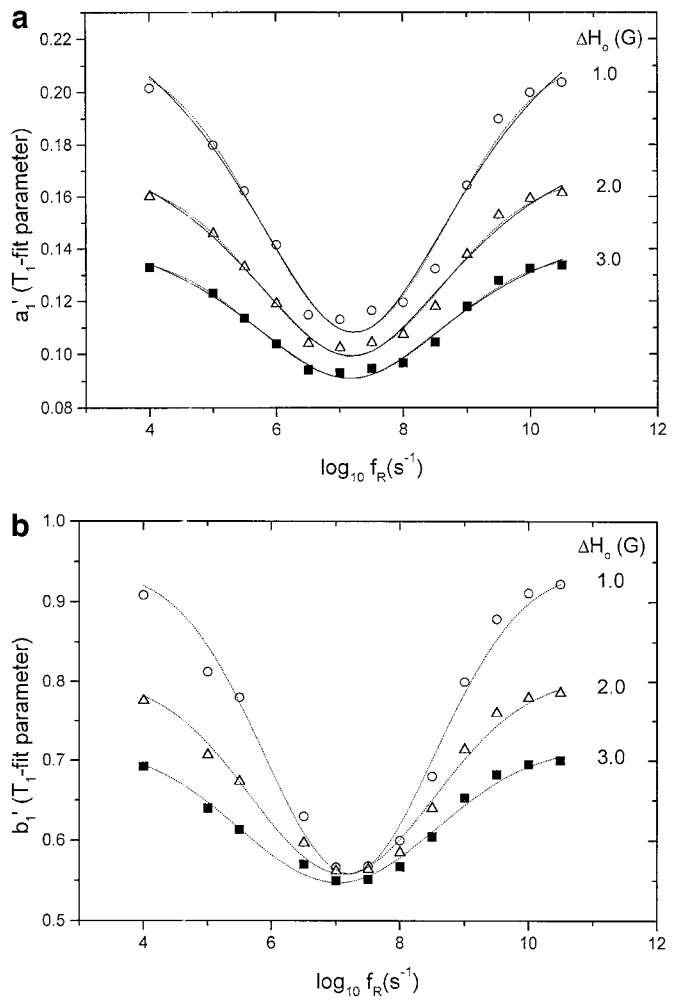

FIG. 4. Simulated dependence on rotational frequency, f_R, of the fit parameters, (a) a_1' and (b) b_1' in Eq. [18] with $m = 2$ and T_1 in μs, for different spin-packet widths, ΔH_0 $(=1/\gamma_e T_{2,0})$, and a modulation frequency of 100 kHz; $H_1 = 0.5$ G. Dotted lines are fits to a Gaussian curve, and solid lines those to a Lorentzian.

TABLE 1

T_1 Calibration of the Intensity Ratio Fitting Parameters in Eq. [18] (with $m = 2$) for a Zeeman Modulation Frequency of 100 kHz, and Rotational Frequencies in the Range 10^4–3.16×10^{10} s^{-1} [a]

f_R (s^{-1})	$\rho_1^{0'}$	a_1'	b_1'
10^4	0.0134–0.0037	0.202–0.133	0.91–0.69
10^5	0.0146–0.0044	0.180–0.123	0.81–0.64
3.16×10^5	0.0147–0.0047	0.162–0.114	0.78–0.61
10^6	0.0129–0.0042	0.142–0.104	0.78–0.62
3.16×10^6	0.0096–0.0031	0.115–0.094	0.63–0.57
10^7	0.0053–0.0022	0.113–0.093	0.56–0.55
3.16×10^7	0.0037–0.0016	0.116–0.094	0.57–0.55
10^8	0.0040–0.0017	0.120–0.097	0.60–0.57
3.16×10^8	0.0053–0.0022	0.134–0.105	0.68–0.60
10^9	0.0076–0.0026	0.164–0.118	0.80–0.65
3.16×10^9	0.0102–0.0031	0.190–0.128	0.88–0.68
10^{10}	0.0120–0.0034	0.200–0.133	0.91–0.69
3.16×10^{10}	0.0127–0.0035	0.204–0.134	0.92–0.70

[a] Results are given for different values of the intrinsic linewidth, ΔH_0, in the range 1–3 G, over the range $T_1 = 0.2$–5.1 μs for which fitting was performed. The microwave field amplitude, H_1, is 0.5 G. Values of a_1' and b_1' are given for T_1 in μs. The adiabatic approximation is used throughout for the simulations.

quencies, with $m = 1.6$ for $\omega_m/2\pi = 100$ kHz and $m = 1.3$ for $\omega_m/2\pi = 25$ kHz. Examples of the dependences on T_1 are shown in Fig. 5, for the amplitudes of both the $M_I = +1$ and $M_I = 0$ hyperfine manifolds. Values of the fit parameters, $\rho_1^{0'}(M_I = +1)$, $a_1'(M_I = +1)$, and $b_1'(M_I = +1)$, for the low-field (i.e., $M_I = +1$) amplitude are given in Tables 3 and 4. The adiabatic approximation was used throughout, but the validity for the rapid motional regime is established later under Experimental Applications.

TABLE 2

T_1 Calibration of the Intensity Ratio Fitting Parameters in Eq. [18] (with $m = 1.3$) for a Zeeman Modulation Frequency of 25 kHz, and Rotational Frequencies in the Range 10^4–3.16×10^{10} s^{-1} [a]

f_R (s^{-1})	$\rho_1^{0'}$	a_1'	b_1'
1×10^4	0.0007–−0.0025	0.0361–0.0303	0.1051–0.0724
1×10^5	0.0010–−0.0023	0.0344–0.0291	0.1041–0.0701
3.16×10^5	0.0013–−0.0021	0.0310–0.0273	0.0928–0.0632
1×10^6	0.0008–−0.0023	0.0273–0.0254	0.0635–0.050
3.16×10^6	−0.0013–−0.0030	0.0278–0.0254	0.0486–0.0430
1×10^7	−0.0030–−0.0034	0.0300–0.0260	0.0490–0.0429
3.16×10^7	−0.0035–−0.0037	0.0309–0.0263	0.0510–0.0438
1×10^8	−0.0032–−0.0036	0.0305–0.0264	0.0542–0.0460
3.16×10^8	−0.0023–−0.0033	0.0309–0.0269	0.0664–0.0529
1×10^9	−0.0012–−0.0030	0.0334–0.0285	0.0868–0.0633
3.16×10^9	−0.0002–−0.0028	0.0355–0.0294	0.0990–0.0673
1×10^{10}	−0.0003–−0.0027	0.0363–0.0302	0.1033–0.0718
3.16×10^{10}	−0.0005–−0.0026	0.0366–0.0305	0.1047–0.0735

[a] Results are given for different values of the intrinsic linewidth, ΔH_0, in the range 1–3 G, over the range $T_1 = 0.2$–5.1 μs for which fitting was performed. The microwave field amplitude, H_1, is 0.5 G. Values of a_1' and b_1' are given for T_1 in μs. The adiabatic approximation is used throughout for the simulations.

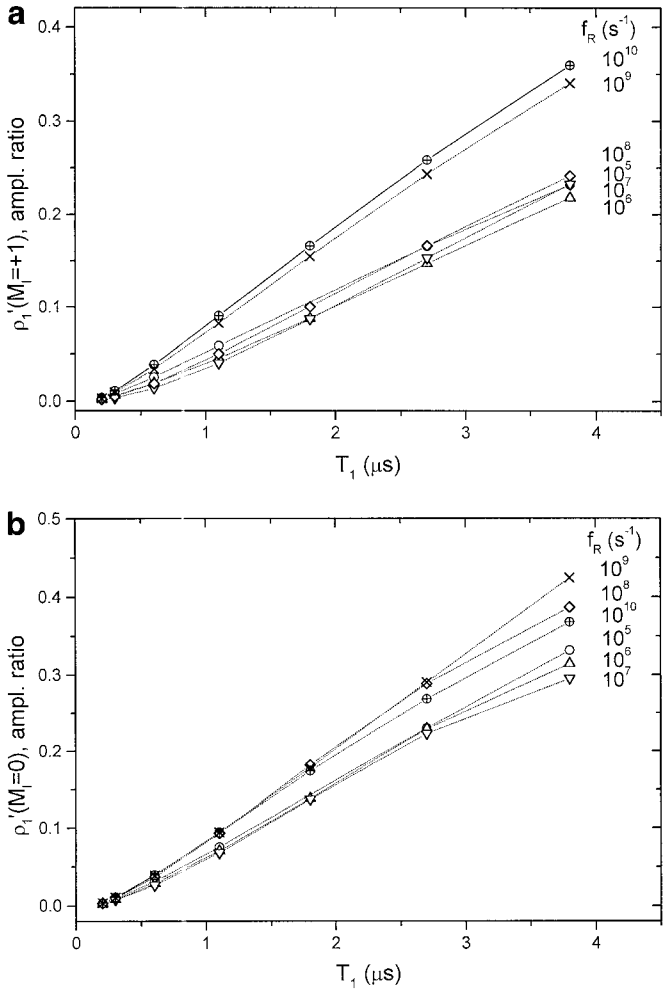

FIG. 5. Simulated dependences on T_1 of the ratio, $\rho_1'(M_I)$, of the amplitudes of (a) the low-field ($M_I = +1$) and (b) the central ($M_I = 0$) hyperfine components of the out-of-phase and in-phase EPR spectra, for different values of rotational frequency f_R and a Zeeman modulation frequency of 25 kHz; $H_1 = 0.5$ G; ΔH_0 ($=1/\gamma_e T_{2,0}$) $= 2.0$ G.

The central part of an EPR spectrum in the slow motion region contains the contributions from the $M_I = \pm 1$ hyperfine components. Nevertheless, amplitudes in this region ($M_I = 0$) are also useful T_1-sensitive parameters. The advantage of this central, $M_I = 0$, region of the spectrum is that it has a larger amplitude than the low- and high-field components. It is seen from Fig. 5 that the sensitivity of this $\rho_1'(M_I = 0)$ amplitude ratio to T_1 is about the same as for $\rho_1'(M_I = +1)$, in the rapid motion region. In the slow motion region, the sensitivity is even greater than for the low-field amplitude ratio, $\rho_1'(M_I = +1)$. Additionally, the $\rho_1'(M_I = 0)$ parameter is only relatively weakly sensitive to inhomogeneous broadening.

In comparison with the integrated intensities, ρ_1', the dependence of the amplitude ratio, $\rho_1'(M_I = +1)$, on f_R is stronger and more asymmetric. This is also true for the individual V_1 and V_1' amplitudes. This is evident in Fig. 5 for the amplitude ratios, and also in the dependences on rotational frequency of the fit parameters, $a_1'(M_I = +1)$ and

TABLE 3

T_1 Calibration of the $M_I = +1$ Amplitude Ratio Fitting Parameters in Eq. [19] (with $m = 1.6$) for a Zeeman Modulation Frequency of 100 kHz, and Rotational Frequencies in the Range 10^4–3.16×10^{10} s^{-1} [a]

f_R (s^{-1})	$\rho_1^{0'}(M_I = +1)$	$a_1'(M_I = +1)$	$b_1'(M_I = +1)$
1×10^4	−0.0060–−0.0116	0.352–0.260	0.629–0.560
1×10^5	0.0007–−0.0065	0.337–0.250	0.623–0.555
3.16×10^5	0.0007–−0.0080	0.269–0.216	0.544–0.487
1×10^6	−0.0001–−0.0076	0.219–0.190	0.555–0.485
3.16×10^6	−0.0060–−0.0095	0.175–0.171	0.473–0.452
1×10^7	−0.0120–−0.0110	0.174–0.169	0.436–0.437
3.16×10^7	−0.0134–−0.0108	0.188–0.177	0.461–0.451
1×10^8	−0.0126–−0.0120	0.251–0.218	0.528–0.498
3.16×10^8	−0.0173–−0.0156	0.370–0.285	0.494–0.481
1×10^9	−0.0169–−0.0171	0.440–0.330	0.500–0.480
3.16×10^9	−0.0151–−0.0175	0.464–0.352	0.507–0.483
1×10^{10}	−0.0141–−0.0176	0.470–0.360	0.508–0.485
3.16×10^{10}	−0.0139–−0.0176	0.470–0.361	0.508–0.486

[a] Results are given for different values of the intrinsic linewidth, ΔH_0, in the range 1–3 G, a peak-to-peak inhomogeneous linewidth of 1.4 G, over the range $T_1 = 0.2$–5.1 μs for which fitting was performed. The microwave field amplitude, H_1, is 0.5 G. Values of $a_1'(M_I = +1)$ and $b_1'(M_I = +1)$ are given for T_1 in μs. The adiabatic approximation is used throughout for the simulations.

$b_1'(M_I = +1)$ in Eq. [19]. The latter are presented in Fig. 6. The asymmetry is explained by the hyperfine- and g-tensor anisotropy. In the absence of motion, and at low rotational frequencies, this results in an anisotropic distribution of resonance fields. At high rotational frequencies this anisotropic distribution is motionally averaged. The dependence of the $\rho_1'(M_I)$ ratio on f_R is determined by the f_R dependences of the individual V_1 and V_1' amplitudes. The V_1' amplitude for $\omega_m/2\pi = 100$ kHz is less dependent on f_R in the slow and intermediate motional regions. At higher rotational frequencies, however, it increases more strongly than does the in-phase amplitude. For the $a_1'(M_I)$ parameter, this dependence is similar to that for $\rho_1'(M_I)$ itself. The minimum in the region $f_R \approx 10^7$ s^{-1} is caused by the stronger effect of spectral diffusion on the V_1 amplitude compared with that on the V_1' amplitude (see Fig. 6a). As for the integrated intensities, going to lower modulation frequencies (i.e., 25 kHz) results in weaker dependences on $T_{2,0}$. This is true both for the amplitude ratio, $\rho_1'(M_I = +1)$, and for the fit parameters, $a_1'(M_I = +1)$ and $b_1'(M_I = +1)$ (compare Tables 3 and 4).

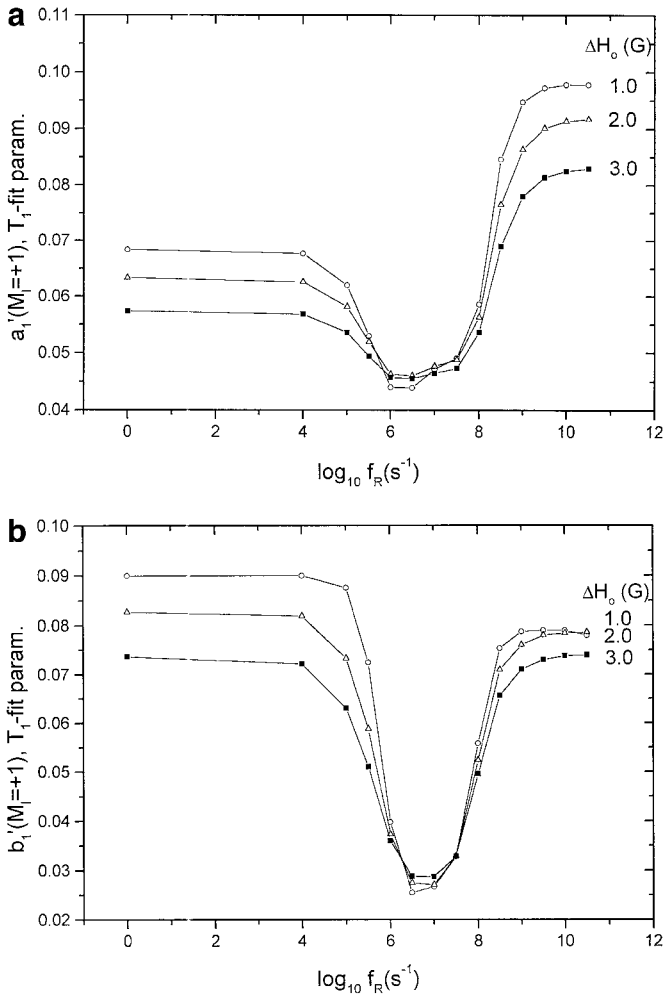

FIG. 6. Dependence on rotational frequency, f_R, of the fit parameters (a) $a_1'(M_I = +1)$ and (b) $b_1'(M_I = +1)$ for the T_1 dependence of the amplitude of the low-field hyperfine line in Eq. [19] with $m = 1.3$ and T_1 in μs, for different values of ΔH_0 ($=1/\gamma_e T_{2,0}$) and a Zeeman modulation frequency of 25 kHz; $H_1 = 0.5$ G.

TABLE 4

T_1 Calibration of the $M_I = +1$ Amplitude Ratio Fitting Parameters in Eq. [19] (with $m = 1.3$) for a Zeeman Modulation Frequency of 25 kHz, and Rotational Frequencies in the Range 10^4–3.16×10^{10} s^{-1} [a]

f_R (s^{-1})	$\rho_1^{0'}(M_I = +1)$	$a_1'(M_I = +1)$	$b_1'(M_I = +1)$
1×10^4	−0.0027–−0.0055	0.0677–0.0568	0.090–0.073
1×10^5	−0.0017–−0.0053	0.0620–0.0540	0.087–0.063
3.16×10^5	−0.0007–−0.0050	0.0530–0.0495	0.072–0.051
1×10^6	−0.0016–−0.0057	0.0440–0.0458	0.040–0.036
3.16×10^6	−0.0059–−0.0074	0.0439–0.0456	0.026–0.028
1×10^7	−0.0084–−0.0082	0.0471–0.0465	0.027–0.029
3.16×10^7	−0.0085–−0.0075	0.0491–0.0473	0.033–0.033
1×10^8	−0.0074–−0.0077	0.0586–0.0537	0.056–0.050
3.16×10^8	−0.0092–−0.0090	0.0846–0.0690	0.075–0.066
1×10^9	−0.0081–−0.0093	0.0948–0.0780	0.079–0.071
3.16×10^9	−0.0071–−0.0093	0.0972–0.0814	0.079–0.073
1×10^{10}	−0.0066–−0.0092	0.0978–0.0826	0.079–0.074
3.16×10^{10}	−0.0065–−0.0092	0.0978–0.0829	0.078–0.074

[a] Results are given for different values of the intrinsic linewidth, ΔH_0, in the range 1–3 G, a peak-to-peak inhomogeneous linewidth of 1.4 G, over the range $T_1 = 0.2$–5.1 μs for which fitting was performed. The microwave field amplitude, H_1, is 0.5 G. Values of $a_1'(M_I = +1)$ and $b_1'(M_I = +1)$ are given for T_1 in μs. The adiabatic approximation is used throughout for the simulations.

Experimental Applications

V_1'- and V_1-EPR spectra were measured for TEMPONE and 5-MSL in glycerol–water mixtures of different viscosities. The measurements were performed with modulation frequencies of 100 and 25 kHz. To extract effective spin–lattice relaxation times from the experimental values of the ρ_1' and $\rho_1'(M_I)$ ratios, calibrations of the fitting parameters for the appropriate rotational correlation times were used (Tables 1–4). Additionally, spectral simulations were performed for fitting to the experimental dependences of ρ_1' and $\rho_1'(M_I = +1)$ ratios on the microwave field intensity, H_1. Rotational correlation times were determined from the conventional V_1-EPR spectra by using calibrations or equations given in Refs. (*12–14*). As noted above, the dependence of the ρ_1', $\rho_1'(M_I = +1)$, and $\rho_1'(M_I = 0)$ ratios on ΔH_0 is relatively unimportant at a modulation frequency of 25 kHz. However, this dependence must be taken into account at $\omega_m/2\pi = 100$ kHz to obtain sufficiently precise T_1 estimates. Residual (i.e., intrinsic) linewidths ($\Delta H_0 = 1/\gamma_e T_{2,0}$) were determined from lineshape simulations of the low-field maximum in the conventional V_1-EPR spectra. Inhomogeneous Gaussian broadening was included explicitly in these simulations.

In the rapid motional regime, rotational correlation times, f_R^{-1}, were estimated from the ratio of low- and high-field lineheights, together with the central linewidth (*14*). The total uncertainty, allowing also for inhomogeneous broadening, is unlikely to exceed 20–30%. In the intermediate and slow motional regimes, the rotational correlation times were determined from the values of the outer hyperfine splitting, relative to rigid limit values from the literature (*13*). The error arising from uncertainties in these values is in the region of 20–30%. However, for small free spin labels in the slow and intermediate regimes, a much greater uncertainty arises from the motional model assumed for the calibrations. This can amount to an uncertainty of 200–300% (*13*). (Note that for spin-labeled macromolecules, the motion is Brownian diffusion and this uncertainty does not exist.) The residual homogeneous linewidths, ΔH_0, were determined from lineshape simulations of the low-field spectral components in the conventional, low-power V_1-EPR spectra. Models appropriate to the different motional regimes were used in the simulations. Allowance was also made for inhomogeneous broadening. It is estimated that the error in ΔH_0 does not exceed 20%.

We have made error estimates for T_1 arising from a 25% uncertainty in linewidth ΔH_0 and a 250% uncertainty in rotational frequency, f_R. This was done for the different motional regimes and for different ranges of T_1. The uncertainty in T_1 from the linewidth measurements increases from 2 to 10% over the range $T_1 = 0.3$–2.5 μs, with $\omega_m/2\pi = 100$ kHz. For a modulation frequency of $\omega_m/2\pi = 25$ kHz, this uncertainty is reduced to 1–4% over the extended range $T_1 = 0.3$–6 μs. In both cases, this applies to rotational frequencies in the range $f_R = 10^6$–10^9 s^{-1}. The uncertainty in f_R is maximum (~250%) for values of $f_R = 10^6$–10^7 s^{-1}. In this range, it results in a maximum uncertainty in T_1 of ~11% for $T_1 = 0.3$–3 μs with $\omega_m/2\pi = 100$ kHz, and of ~10% for $T_1 = 0.3$–6 μs with $\omega_m/2\pi = 25$ kHz. For higher rotational frequencies, the uncertainty in f_R is much lower and correspondingly the uncertainty in T_1 is reduced. For $f_R = 5 \times 10^7$–5×10^9 s^{-1}, an uncertainty of 50% in f_R results in an uncertainty in T_1 of ~2% (for $T_1 = 0.3$–3 μs with $\omega_m/2\pi = 100$ kHz), or ~1% (for $T_1 = 0.3$–6 μs with $\omega_m/2\pi = 25$ kHz).

The above error estimates were made for T_1 determinations from the integrated intensity ratio, ρ_1'. For the amplitude ratios, $\rho_1'(M_I)$, the corresponding errors in T_1 are of the same order of magnitude. However, unlike the integrated intensity ratios, the measured amplitude ratios also depend on the degree of Gaussian inhomogeneous broadening. Simulations using the present methods show that the effects of inhomogeneous broadening on the amplitude ratios are qualitatively similar to those for the no motion case (see Ref. *6*). The accuracy of determining the inhomogeneous broadening for simulations is similar to that for the homogeneous broadening. This amounts to an uncertainty of 20–30%. For an uncertainty in inhomogeneous broadening of 25%, with $\Delta H_0 = 1$ G, the uncertainty in T_1 determination from the amplitude ratio is 3.5–7%, depending on the range of T_1. This applies to low and high rotational frequencies, i.e., $f_R = 10^6$ or 10^9–10^{10} s^{-1}. At intermediate rotational frequencies ($f_R = 10^8$–10^7 s^{-1}), the above uncertainty in T_1 decreases to 1–1.5%. This is because rotational relaxation broadening dominates in this regime. Correspondingly, the amplitude ratios are also less sensitive to inhomogeneous broadening at larger intrinsic homogeneous linewidths ($\Delta H_0 > 1$ G).

1. TEMPONE in glycerol–water mixtures. The glycerol content and temperature were adjusted to obtain rotational correlation times corresponding to the slow ($\tau_R \cong 33$ ns), intermediate ($\tau_R \cong 10$ ns), and rapid ($\tau_R \cong 0.5$, 0.67, and 0.9 ns) motional regimes. The fit parameters presented in Tables 1–4 were obtained with the adiabatic approximation for the whole range of f_R. To check the accuracy of such an approach for the rapid motion region, additional simulations were performed that did not rely on this approximation. These further simulations used: (i) Eqs. [12]–[15] for the rotational contribution to the linewidth from time-dependent perturbation theory with the full spin Hamiltonian, or (ii) the same equations without the nuclear frequency-dependent terms. Experimental dependences of the ρ_1' and $\rho_1'(M_I = +1)$ ratios on H_1 are given for TEMPONE in 100% glycerol at 30°C in Fig. 7a. Those for TEMPONE in 80% glycerol at 20°C are given in Fig. 7b. The simulated dependences of these parameters on H_1, calculated with method (i) and also with the adiabatic approximation, are given in the same figures. When values of ΔH_0 were determined consistently from simulations with the corresponding lineshape equations, the values obtained for T_1 from the two approximations were closely similar (see Figs. 7a and 7b). The values determined for ΔH_0 from the two models are 0.75 and

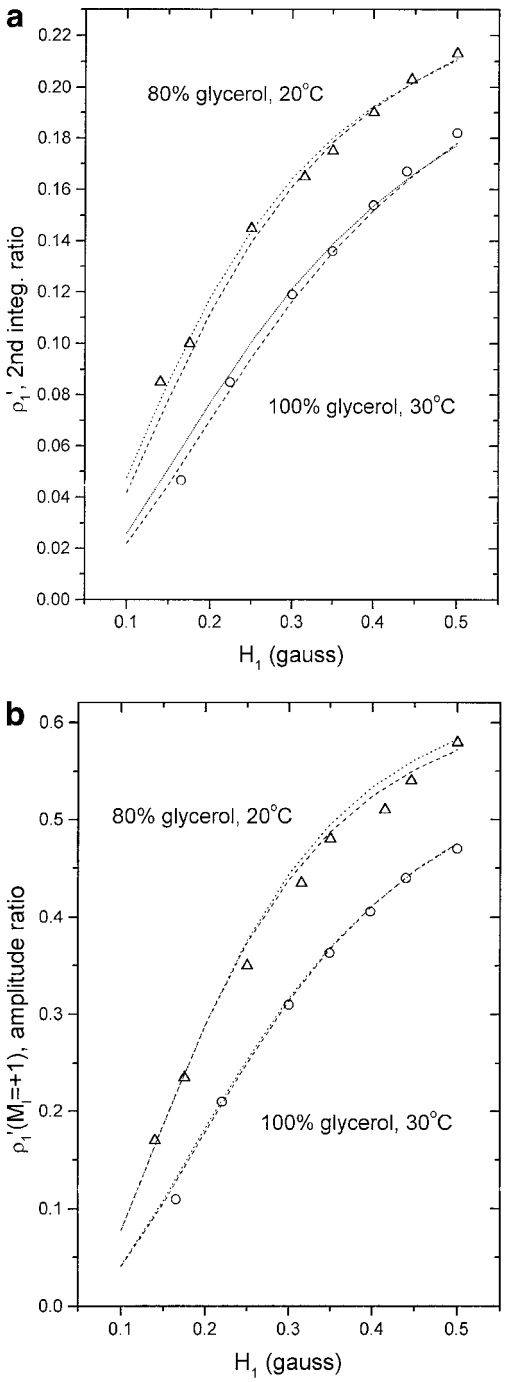

FIG. 7. Experimental and simulated dependences on microwave field strength, H_1, of the ratio of (a) the integrated intensities, ρ_1', and (b) the low-field amplitudes, $\rho_1'(M_I = +1)$, of the first-harmonic out-of-phase and in-phase EPR spectra, for the TEMPONE radical in 100% glycerol at 30°C (○) and 80% glycerol at 20°C (△). The Zeeman modulation frequency is 100 kHz. Simulations were performed with the adiabatic (dotted lines) and second-order perturbation (dashed lines) models. The best-fit values of rotational frequency and spin-packet width to the linear V_1-EPR spectra for the two models are $f_R = 1.1 \times 10^9\ s^{-1}$, $\Delta H_0 = 0.95$ and 0.75 G, respectively, for 100% glycerol at 30°C, and $f_R = 2.1 \times 10^9\ s^{-1}$, $\Delta H_0 = 0.55$ and 0.42 G, respectively, for 80% glycerol at 20°C. The T_1 values determined from the simulated H_1 dependencies are (a) 2.0 and 2.2×10^{-6} s, and (b) 1.6 and 1.7×10^{-6} s, respectively, for 100% glycerol at 30°C, and (a) 2.4 and 2.6×10^{-6} s, and (b) 1.75 and 1.85×10^{-6} s, respectively, for 80% glycerol at 20°C.

0.95 G for TEMPONE in 100% glycerol, and 0.42 and 0.55 G for TEMPONE in 80% glycerol, respectively.

Satisfactory fits for the dependence of both ρ_1' and $\rho_1'(M_I = +1)$ on H_1, and agreement between the values deduced for T_1, are obtained from the two approximations. This result is of considerable importance. It means that the calibrations in Tables 1–4 can be used with confidence throughout the entire range of rotational frequencies. However, the absolute values of T_1 determined from the amplitudes are somewhat lower than those obtained from the integrated intensities. The effect of inhomogeneous broadening is insignificant for TEMPONE because the inhomogeneous linewidth is very small for this nitroxide (0.215 G peak-to-peak) (*15*). The slight difference between the T_1 values may be attributed to differences in T_1 (and possibly in ΔH_0) for the three hyperfine components.

The spin relaxation parameters of the TEMPONE radical in different motional regimes were measured in 90% glycerol at various temperatures (20, −1, and −30°C). At lower temperatures, one predicts that the T_1 values lie outside the region of optimum T_1 sensitivity ($T_1 \leq 4\ \mu s$) for a modulation frequency of 100 kHz (see Fig. 2). Therefore, these measurements were performed with a modulation frequency of 25 kHz. The values of T_1 for the intermediate and slow motional regimes were determined from the ρ_1' and $\rho_1'(M_I = +1)$ ratios measured at two values of H_1, 0.4 and 0.5 G, by using the calibrations in Tables 2 and 4. These values, together with the spin-packet widths (ΔH_0), are given in Table 5. The T_1 values determined from the ratio of integrated intensities agree satisfactorily for the independent measurements with $H_1 = 0.4$ and 0.5 G. Similar agreement is observed for the T_1 values determined from the amplitude ratios, $\rho_1'(M_I = +1)$. However, the latter T_1 values are somewhat lower than the former ones, as noted above for TEMPONE in 100 and 80% glycerol solutions at 20°C.

Consistency is obtained between the values of T_1 determined by fitting the H_1 dependence for TEMPONE in 90% glycerol at 20°C, and those obtained from the calibrations given in Tables 1 and 2 for measurements with a different (i.e., 100 kHz) modulation frequency (see Table 5). At a modulation frequency of 25 kHz, the T_1 values obtained from the adiabatic approximation and from simulation method (i) again both agree, as found already at a modulation frequency of 100 kHz. These results serve as further experimental validation of the simulation methods used. Also, the values of T_1 obtained for TEMPONE in 80% glycerol at 20°C are very close to those obtained for small spin labels with similar rotational correlation times by saturation recovery methods (*16*). The value of T_1 obtained for TEMPONE at a rotational correlation time of $\tau_R = 10$ ns (see Table 5) is close to that estimated from the progressive saturation parameter and linewidth measurements for a similar small spin label in glycerol–water. For 4-hydroxy-2,2,6,6-tetramethylpiperidine-*N*-oxyl at $\tau_R = 8.5 \pm 0.5$ ns we determined a value of $T_1 = 4.8 \pm 0.6\ \mu s$ by progressive saturation (*10*). More direct comparison with progressive sat-

TABLE 5

Spin Relaxation Properties of TEMPONE in Glycerol–Water Mixtures of Different Viscosities Deduced from the Spectral Parameters of the Out-of-Phase and In-Phase First-Harmonic EPR Spectra at Modulation Frequencies of 100 and 25 kHz

Glycerol (%)	T (°C)	τ_R (ns)	ΔH_0 (G)	$\omega_m/2\pi$ (kHz)	H_1 (G)	ρ_1'	T_1 (μs)	$\rho_1'(M_1)$	T_1 (μs)
80	20	0.48	0.55	100	0.15–	$f(H_1)$[a]	2.4	$f(H_1)$[a]	1.75
			0.42[b]		0.5		2.6[b]		1.85[b]
100	30	0.9	0.95	100	0.15–	$f(H_1)$[a]	2.0	$f(H_1)$[a]	1.6
			0.75[b]		0.5		2.2[b]		1.7[b]
90	20	0.67	0.9	100	0.5	0.195	2.85	0.62	2.35
			0.7[b]			0.195	3.0[b]		2.45[b]
90	20	0.67	0.9	25	0.15–	$f(H_1)$[a]	3.0	$f(H_1)$[a]	2.7
			0.7[b]		0.5		3.1[b]		2.8[b]
90	−1	10	1.8	25	0.4	0.148	5.4	0.262	4.8
					0.5	0.173	5.5	0.309	4.9
90	−30	33	2.0	25	0.4	0.17	6.5	0.278	5.7
					0.5	0.218	6.9	0.355	5.8

[a] T_1 values are obtained from fitting the intensity (ρ_1') or amplitude ($\rho_1'(M_1)$) ratios as a function of H_1, over the range given.
[b] Values determined from time-dependent perturbation theory. All other values are obtained by using the adiabatic approximation.

uration experiments for the fast and very slow motional regimes can be found in our previous paper (*6*).

Table 5 shows that it is sufficient to perform V_1'-EPR measurements at a single high microwave field intensity. Consistent values are obtained for T_1 from single-point measurements at $H_1 = 0.4$ G and $H_1 = 0.5$ G. These values are also consistent with those obtained by fitting the complete H_1 dependence. Routinely, therefore, V_1'-EPR measurements would be made at $H_1 = 0.4$ or 0.5 G, and the calibrations of Tables 1–4 used.

2. 3-Maleimide proxyl in glycerol–water mixtures. Similar T_1 measurements were performed for the 5-MSL spin label in 90% glycerol–water mixtures, with a modulation frequency of 25 kHz. Again measurements were made in the rapid, intermediate, and slow motional regimes. For 5-MSL, these motional regimes correspond to higher temperatures than for TEMPONE (40, 20, and −2°C). The T_1 values, as well as homogeneous linewidths and rotational correlation times, are given in Table 6. For this spin label the T_1 values obtained from the integrated intensities agree satisfactorily with those determined from the amplitude ratios. The absolute values of T_1 are found to be higher for MSL than for TEMPONE, at the same glycerol content and temperatures. The value of T_1 at −2°C can be compared with the value of 6.6 μs for this label bound to hemoglobin in a 90% glycerol–water mixture at 0°C (*4*).

CONCLUSIONS

The advantages of the first-harmonic out-of-phase V_1'-EPR method that were previously established for CW T_1 determinations are insensitivity to T_2, favorable signal strength, and ability to tune the range of sensitivity to T_1 by varying the Zeeman modulation frequency (*6*). These results, however, were obtained only for spin labels in the very fast or very slow motional regimes and by theoretical simulations for single-line spectra. The present work extends the validity of these conclusions by simulations of the complete nitroxide spin-label V_1'-EPR spectrum and by investigating the full range of nitroxide spin-label rotational correlation times. An important further finding is that T_1 relaxation time determinations by the V_1'-EPR method are less affected by rotational motion of the spin label

TABLE 6

Spin Relaxation Properties of 3-Maleimide Proxyl Spin Label in Glycerol–Water Mixtures of Different Viscosities Deduced from the Spectral Parameters of the Out-of-Phase and In-Phase First-Harmonic EPR Spectra

Glycerol (%)	T (°C)	τ_R (ns)	ΔH_0 (G)	H_1 (G)	ρ_1'	T_1 (μs)	$\rho_1'(M_1)$	T_1 (μs)
90	+40	1.1	1.6	0.4	0.068	2.5	0.195	2.4
			1.3[a]			2.5[a]		2.5[a]
90	+20	10	2.0	0.4	0.1	3.7	0.202	3.7
				0.5	0.14	4.2	0.266	4.1
90	−2	33	2.1	0.4	0.15	5.5	0.283	5.6

Note. The modulation frequency is 25 kHz.
[a] Values determined from time-dependent perturbation theory. All other values are obtained by using the adiabatic approximation.

than are other nonlinear methods. This result reinforces the usefulness of V'_1-EPR as a "pure" T_1-sensitive display, as was suggested originally in Ref. (*7*). Particularly, this holds for Zeeman modulation frequencies in the region around 25 kHz that are appropriate for use with spin labels. Calibrations that are presented for the T_1 dependence of the intensity and amplitude ratios for different correlation times considerably improve the precision of the method at modulation frequencies in the standard range around 100 kHz.

The results presented here should help to establish this new nonlinear CW EPR method on a firm basis, and to stimulate further applications. Its use in studying paramagnetic relaxation enhancement of spin-labeled fatty acids bound to bovine serum albumin will be reported elsewhere. One further extension that can be envisaged is to exploit the dependence of T_1 sensitivity on modulation frequency to study heterogeneous systems with different T_1 values that give unresolved or overlapped conventional EPR spectra.

ACKNOWLEDGMENTS

This work was supported by the Deutsche Forschungsgemeinschaft and by Grant 98-03-33270 of the Russian Foundation for Basic Research.

REFERENCES

1. C. Altenbach, T. Marti, H. G. Khorana, and W. L. Hubbell, Transmembrane protein structure: Spin labelling of bacteriorhodopsin mutants, *Science* **248,** 1088–1092 (1990).
2. W. L. Hubbell, A. Gross, R. Landgren, and M. A. Lietzow, Recent advances in site-directed spin labeling of proteins, *Curr. Opin. Struct. Biol.* **8,** 649–656 (1998).
3. D. Marsh, Progressive saturation and saturation transfer ESR for measuring exchange processes of spin labelled lipids and proteins in membranes, *Chem. Soc. Rev.* **22,** 329–335 (1993).
4. D. D. Thomas, L. R. Dalton, and J. S. Hyde, Rotational diffusion studied by passage saturation transfer of electron paramagnetic resonance, *J. Chem. Phys.* **65,** 3006–3024 (1976).
5. T. Páli, V. A. Livshits, and D. Marsh, Dependence of saturation-transfer EPR intensities on spin–lattice relaxation, *J. Magn. Reson. B* **113,** 151–159 (1996).
6. V. A. Livshits, T. Páli, and D. Marsh, Spin relaxation measurements using first-harmonic out-of-phase EPR signals, *J. Magn. Reson.* **134,** 113–123 (1998).
7. J. S. Hyde and D. D. Thomas, New EPR methods for the study of very slow motion: Application to spin-labeled hemoglobin, *Ann. N.Y. Acad. Sci.* **222,** 680–692 (1973).
8. P. Fajer and D. Marsh, Microwave and modulation field inhomogeneities and the effect of cavity *Q* in saturation transfer ESR spectra. Dependence on sample size, *J. Magn. Reson.* **49,** 212–224 (1982).
9. M. A. Hemminga, P. A. de Jager, D. Marsh, and P. Fajer, Standard conditions for the measurement of saturation transfer ESR spectra, *J. Magn. Reson.* **59,** 160–163 (1984).
10. V. A. Livshits, T. Páli, and D. Marsh, Relaxation time determinations by progressive saturation EPR: Effects of molecular motion and Zeeman modulation for spin labels, *J. Magn. Reson.* **133,** 79–91 (1998).
11. R. C. McCalley, E. J. Shimshick, and H. M. McConnell, The effect of slow rotational motion on paramagnetic resonance spectra, *Chem. Phys. Lett.* **13,** 115–119 (1972).
12. J. Israelachvili, J. Sjösten, L. E. G. Eriksson, M. Ehrström, A. Gräslund, and A. Ehrenberg, ESR spectral analysis of the molecular motion of spin labels in lipid bilayers and membranes based on a model in terms of two angular motional parameters and rotational correlation times, *Biochim. Biophys. Acta* **382,** 125–141 (1975).
13. J. H. Freed, Theory of slow tumbling ESR spectra of nitroxides, *in* "Spin Labelling. Theory and Applications" (L. J. Berliner, Ed.), pp. 53–132, Academic Press, New York (1976).
14. S. Schreier, C. F. Polnaszek, and I. C. P. Smith, Spin labels in membranes. Problems in practice, *Biochim. Biophys. Acta* **515,** 375–436 (1978).
15. B. L. Bales, Inhomogeneously broadened spin-label spectra, *in* "Biological Magnetic Resonance" (L. J. Berliner and J. Reuben, Eds.), Vol. 8, Chap. 2, pp. 77–130, Plenum Press, New York/London (1989).
16. P. W. Percival and J. S. Hyde, Saturation-recovery measurements of spin–lattice relaxation times of some nitroxides in solution, *J. Magn. Reson.* **23,** 249–257 (1976).